Philosophical Magazine
Publication details, including instructions for authors and subscription information:
http://www.tandfonline.com/loi/tphm20

Multiscale, multiphysics geomechanics for geodynamics applied to buckling instabilities in the middle of the Australian craton

Klaus Regenauer-Lieb[ab], Manolis Veveakis[a], Thomas Poulet[ac], Martin Paesold[d], Gideon Rosenbaum[e], Roberto F. Weinberg[f] & Ali Karrech[g]

[a] School of Petroleum Engineering, The University of New South Wales, Sydney, NSW 2052, Australia

[b] School of Earth & Environment, The University of Western Australia, M051, 35 StirlingHwy, Crawley, WA 6009 Australia

[c] CSIRO, 26 Dick Perry Ave., Kensington, WA, 6151 Australia

[d] School of Mathematics and Statistics, The University of Western Australia, M051, 35 StirlingHwy, Crawley, WA 6009 Australia

[e] School of Earth Sciences, University of Queensland, Brisbane, Queensland, 4072, Australia.

[f] School of Geosciences, Monash University, Building 28, Clayton, Victoria, 3800, Australia.

[g] School of Civil and Resource Engineering The University of Western Australia, M051, 35 StirlingHwy, Crawley, WA 6009 Australia

Published online: 17 Aug 2015.

To cite this article: Klaus Regenauer-Lieb, Manolis Veveakis, Thomas Poulet, Martin Paesold, Gideon Rosenbaum, Roberto F. Weinberg & Ali Karrech (2015): Multiscale, multiphysics geomechanics for geodynamics applied to buckling instabilities in the middle of the Australian craton, Philosophical Magazine, DOI: 10.1080/14786435.2015.1066517

To link to this article: http://dx.doi.org/10.1080/14786435.2015.1066517

Philosophical Magazine, 2015
http://dx.doi.org/10.1080/14786435.2015.1066517

Taylor & Francis
Taylor & Francis Group

Multiscale, multiphysics geomechanics for geodynamics applied to buckling instabilities in the middle of the Australian craton

Klaus Regenauer-Lieb[ab*], Manolis Veveakis[a], Thomas Poulet[ac], Martin Paesold[d], Gideon Rosenbaum[e], Roberto F. Weinberg[f] and Ali Karrech[g]

[a] *School of Petroleum Engineering, The University of New South Wales, Sydney, NSW 2052, Australia;* [b] *School of Earth & Environment, The University of Western Australia, M051, 35 Stirling Hwy, 6009 Crawley, WA, Australia;* [c] *CSIRO, 26 Dick Perry Ave., 6151 Kensington, WA, Australia;* [d] *School of Mathematics and Statistics, The University of Western Australia, M051, 35 Stirling Hwy, 6009 Crawley, WA, Australia;* [e] *School of Earth Sciences, University of Queensland, Brisbane, Queensland 4072, Australia;* [f] *School of Geosciences, Monash University, Building 28, Clayton, Victoria 3800, Australia;* [g] *School of Civil and Resource Engineering The University of Western Australia, M051, 35 Stirling Hwy, 6009 Crawley, WA, Australia*

(*Received 3 November 2014; accepted 4 May 2015*)

We propose a new multi-physics, multi-scale Integrated Computational Materials Engineering framework for 'predictive' geodynamic simulations. A first multiscale application is presented that allows linking our existing advanced material characterization methods from nanoscale through laboratory-, field and geodynamic scales into a new rock simulation framework. The outcome of our example simulation is that the diachronous Australian intraplate orogenic events are found to be caused by one and the same process. This is the non-linear progression of a fundamental buckling instability of the Australian intraplate lithosphere subject to long-term compressive forces. We identify four major stages of the instability: (1) a long wavelength elasto-visco-plastic flexure of the lithosphere without localized failure (first 50 Myrs of loading); (2) an incipient thrust on the central hinge of the model (50–90 Myrs); (3) followed by a secondary and tertiary thrust (90–100 Myrs) 200 km away to either side of the central thrust; (4) a progression of subsidiary thrusts advancing towards the central thrust (>100 Myrs). The model is corroborated by multiscale observations which are: nano–micro CT analysis of deformed samples in the central thrust giving evidence of cavitation and creep fractures in the thrust; mm–cm size veins of melts (pseudotachylite) that are evidence of intermittent shear heating events in the thrust; and 1–10 km width of the thrust – known as the mylonitic Redbank shear zone – corresponding to the width of the steady state solution, where shear heating on the thrust exactly balances heat diffusion.

Keywords: multiscaling; multiphysics; microstructure; homogenization; complex systems; fluid dynamics; solid mechanics; geomechanics

1. Introduction

Current generations of geodynamic models of lithosphere deformation are capable of quantitatively describing individual geological observations. However, they are not designed

*Corresponding author. Email: klaus@unsw.edu.au

to explain – with one and the same theory – fundamental observations in nature. There is therefore uncertainty in understanding the basic physics that drive principal geodynamic processes. The geodynamic community is still debating the source mechanisms for well-documented dynamic processes such as: subduction initiation, large scale continental deformation, oroclinal bending, the phenomenon of slow earthquakes, seismic instabilities, episodic tremor and slip, intraplate volcanism and lastly intraplate deformation. Classical models require special pleading such as pre-existing zones of weakness, or imposed strain weakening laws, or laboratory-derived rate and state friction laws to describe individual lithosphere deformation processes. We propose here an alternative approach that we call 'unconventional' (=multiphysics, multiscale) geomechanics. It offers (potentially) a unified 'predictive' approach. Although we only provide the first application to the paradox of intraplate deformation, the framework should ultimately be capable of (i) accurately describing the processes that lead or have led to the formation of the above-described phenomena, hence defining their geometric and quantitative relationship to their source rocks and dynamic microphysical engines (ii) allowing physics-based exploration with geophysical/geological inversion methods coupled to the forward models; (iii) understand the stability/activation of fault zones in the present day stress field; (iv) develop new ways of predicting instabilities for hazard assessment and (v) provide a quantitative method for uncovering Earth's resources with less energy and water requirement for their production.

To this end, we propose to use a new multiphysics, multiscale Integrated Computational Materials Engineering (ICME) framework for 'predictive' geodynamic simulations. We also propose to extend this approach in the future for the resource industry to improve exploration, characterization and even stimulation of conventional and unconventional reservoir materials. ICME is an emerging discipline that has been successfully used in the automotive, aerospace and nuclear industry to integrate computational materials science tools into a multiscale system. It has been heralded as a transformational discipline by the National Academy of Sciences [1] and is based on integration of materials information, captured in computational tools, with engineering product performance analysis and production-process simulation.

2. Multiscale modelling of Earth materials

We describe a series of instability mechanisms relying on the multiphysics feedback in continuity and momentum equilibrium caused by the thermodynamic fluxes of a creeping solid. The mechanism incorporates the volume change associated with a phase transformation, where the rate of reaction is dictated by the rate of creeping and the associated heating rate on the background of slow deformation of the solid. We consider the equilibrium equations of continuity (mass), linear and angular momentum, energy and entropy. For the first four equilibrium equations, we use the standard formulations and emphasize the important role of the deformational power and its role on controlling the time-dependent material behaviour. In this multiscale formulation, it forms the master equation from which the constitutive relationships can be derived. We recapitulate first the basic elements of the approach. For a complete formulation we refer to [2,3].

2.1. *Thermomechanics*

We first look at a thermomechanical recast of classical continuum mechanics [4] which does not incorporate temperature or time evolution. This theory is also known as the

continuum thermomechanics [5]. In this theory, the isothermal deformational power is identified as:

$$\sigma_{ij}\dot{\epsilon}_{ij} \equiv \tilde{W} = \dot{\Psi} + \tilde{\Phi}, \tag{1}$$

where Ψ is the Helmholtz free energy density, $\tilde{W}$ is the rate of working of the applied stress and $\tilde{\Phi}$ is the rate of dissipation, which must be positive (Clausius–Duhhem inequality). The overdot refers to a complete (i.e. integrable) time differential. The over-tilde refers to an incomplete time differential, which introduces path dependence and needs to be integrated with a Feynman integral over all possible paths. This issue lies at the heart of the uncertainty principles in thermodynamics for which the postulates of minimum and maximum entropy production provide useful bounds as a generalized form of the limit analysis and design, i.e. upper and lower bound principles of classical plasticity theory [6,7].

The thermodynamic approach also allows a convenient extension of the classical definition of stress and strain that incorporates multiphysics internal processes. These generalized stresses and strains are also known as the thermodynamic forces and fluxes [8] and turn out to be the partial Legendre duals of the thermodynamic potential functions. They are obtained as the partial derivative of the Helmholtz free energy $\Psi_{(\epsilon_{ij},\alpha^k)}$ and its Legendre transform the Gibbs free energy $G_{(\epsilon_{ij},\alpha^k)}$. These generalized stresses and strains consider in addition to the classical strain ϵ_{ij} other internal microstrains α^k, the superscript k refers to the kth process describing the multiphysics across scales.

In this formulation, we recover the Cauchy stress as a special case:

$$\sigma_{ij} \equiv \frac{\partial \Psi_{(\epsilon_{ij},\alpha^k)}}{\partial \epsilon_{ij}} \tag{2}$$

and the classical Lagrangian strain becomes

$$\epsilon_{ij} \equiv \frac{\partial G_{(\epsilon_{ij},\alpha^k)}}{\partial \sigma_{ij}}. \tag{3}$$

Note that the above Legendre duals of the thermodynamic potential functions are conjugate variables. These relations provide reversibility of the elastic deformation with frozen dissipative processes. Using Equation (1) we obtain

$$\sigma_{ij}\dot{\epsilon}_{ij} = \frac{\partial \Psi}{\partial \epsilon_{ij}}\dot{\epsilon}_{ij} + \frac{\partial \Psi}{\partial \alpha^k}\dot{\alpha}^k + \frac{\partial \tilde{\Phi}}{\partial \dot{\alpha}^k}\dot{\alpha}^k, \tag{4}$$

where we recognize additional terms through the generalized stresses and strains. These additional terms form the basis of Ziegler's orthogonality rule [5] where for maximum entropy production, following equality must hold:

$$\frac{\partial \Psi}{\partial \alpha^k}\dot{\alpha}^k = \frac{\partial \tilde{\Phi}}{\partial \dot{\alpha}^k}\dot{\alpha}^k. \tag{5}$$

By differentiating Equation (3) with respect to time, we also recover the additive decomposition of elastic (first term), plastic or creep microstrains α^k (second term):

$$\dot{\epsilon}_{ij} = \frac{\partial^2 G}{\partial \sigma_{ij}^2}\dot{\sigma}_{ij} + \frac{\partial^2 G}{\partial \sigma_{ij}\partial \alpha^k}\dot{\alpha}^k = \dot{\epsilon}_{ij}^{el} + \dot{\epsilon}_{ij}^{pl} + \dot{\epsilon}_{ij}^{creep}. \tag{6}$$

The second term is a plastic strain rate if the micro process causing the strain can be simplified to be time independent (classically dealt within the theory of Solid Mechanics) and it is a creep strain if the process has important time dependence (classically dealt within the theory of fluid dynamics). The classical theory of thermomechanics is not written to deal with the time-dependent problem in a self-consistent way and we need to expand the approach and relax the classical assumption of isothermal deformation of thermomechanics [9] to derive an evolution law from the thermodynamic potential function.

2.2. *Fluid dynamic evolution law*

For the derivation of the time-dependent evolution law, we must add temperature dependence and consider the complete differentiation of the first law with respect to time. As the derivation is easily accessible in the literature (a recent summary can be found in Ref. [10]), we only summarize the key elements. Firstly, the dissipation function in Equation (1) can no longer be treated as rate independent and we need to consider rate effects through temperature-dependent dissipation $\tilde{\Phi} = T\tilde{S}^{irr}$, where $\tilde{S}^{irr}$ is the internal entropy production (dissipation) of the irreversible microprocesses. Second, an additional term also appears that tracks the bulk entropy of the system as a function of the temperature evolution $S\dot{T}$ where $\partial S \equiv \partial Q/T$. Equation (1) now writes

$$\tilde{W} = \dot{\Psi} + S\dot{T} + T\tilde{S}^{irr}. \tag{7}$$

The temperature evolution equation can be derived from this by considering 2nd law. We arrive at the master energy evolution equation:

$$\frac{D^{(m)}T}{Dt} = \kappa_T \frac{\partial^2 T}{\partial x_k^2} + \frac{\delta_{loc}}{\rho C} \pm \frac{r_k}{\rho C} \pm \rho T \frac{\partial^2 \psi}{\partial T \partial \alpha^k}\dot{\alpha}^k, \tag{8}$$

where κ_T is thermal diffusivity, ρ the density and $C \equiv -T\frac{\partial^2 \psi}{\partial T^2}$ the specific heat. The source/sink term r_k represents volumetric heat production due to chemical reactions or other sources such as electric currents (Joule heating) or radioactive decay. The fraction of the local dissipation that appears as heat is the shear heating term δ_{loc}. It receives feedback from the last term $\rho_m T\frac{\partial^2 \psi}{\partial T \partial \alpha^k}\dot{\alpha}^k$ which represents a generalized latent heat release that can be endothermic (negative = heat sink) or exothermic (positive = heat source). The shear heating term is:

$$\delta_{loc} = \sigma_{ij}\dot{\epsilon}_{ij}^{in} - \frac{\partial \psi}{\partial \alpha^k}\dot{\alpha}^k \geq 0, \tag{9}$$

where the second term describes the power that is stored in the microstructure, which is not available for shear heating.

3. Solid vs. fluid dynamic multiscale formulation

A complete thermodynamic description of the multiscale and multiphysics problem based on integrating the above-described evolution laws over all possible paths and multiphysics feedbacks is difficult to achieve. We must therefore look for possible simplifications. Can we come up with a hybrid scheme where the complex material evolution laws from the smaller scale can be used as average outputs for modelling at the larger scale? We extend

here an approach proposed for modelling the fluid dynamics of solid mechanical shear zones [11]. This scheme relies on a staggered integration of time-dependent material properties to arrive at a simplified solid mechanical problem for the next scale up.

4. Solid and fluid dynamics combined

Perzyna's [13] overstress formulation allows a combination of classical time-symmetric (quasistatic) plasticity theory with a time-dependent fluid dynamic solution. For this we assume the following definition of strain as a continuous function of the effective stress σ'_{ij} and the material temperature T and its internal variables α^k:

$$\dot{\epsilon}^{in}_{ij} = f(\sigma'_{ij}, T, \alpha^k). \tag{10}$$

The time dependence is implicit in the evolution laws of α^k and T as expressed in Equation (8). By expanding Equation (10) around the effective yield stress σ'_Y we obtain

$$\dot{\epsilon}^{in}_{ij} = f' \left(\frac{\bar{\sigma}_{ij}}{\sigma'_n}\right) + \sum_{m\geq 2} f^{(m)} \left(\frac{\bar{\sigma}_{ij}}{\sigma'_n}\right)^m, \tag{11}$$

where $\bar{\sigma}_{ij} = \sigma'_{ij} - \sigma_Y$, σ'_n a reference stress and $f^{(m)} = \frac{1}{m!} \left| \frac{d^m f(\sigma'_{ij}, T, \alpha^k)}{d\sigma'^m_{ij}} \right|_{\sigma'_{ij}=\sigma'_Y}$.

We recover the classical time-independent plastic constitutive behaviour from the first order of the Taylor expansion. For this formulation, we may define the value of the effective stress at yield σ'_Y. The higher order terms describe the solid-fluid transition with a non-linear fluid dynamic visco-plastic behaviour. We recover the classical overstress formulation $\bar{\sigma}_{ij} = \sigma'_{ij} - \sigma'_Y$ of Ref. [13], which describes the stress evolution following the phase transition inside the zone that has encountered plastic deformation.

We therefore identify the second term of Equation (11) as the fluid dynamic visco-plastic strain $\dot{\epsilon}^{vp}_{ij}$ which is activated at overstress:

$$\dot{\epsilon}^{vp}_{ij} = \sum_m f^{(m)} \left(\frac{\bar{\sigma}'_{ij}}{\sigma'_n}\right)^m \quad \text{when} \quad \bar{\sigma}_{ij} > 0, \tag{12}$$

where $f^{(m)}$ is a reference strain rate.

5. Multiscale instabilities

Instabilities in Earth and Planetary sciences are known to take place over a wide range of scales from nuclear instabilities to supernova explosions. They are based on coupling of multiscale and multiphysics processes which from an energetic perspective can generically be described by the solid-fuel model of combustion theory [14]. They can cascade from time scales that range from femtoseconds to billions of years associated with spatial scales that range from subnanometer to billions of light years. Earth Sciences and Astronomy are studying the dynamics of these multiscale phenomena via the use of high-performance simulations. As these multiscale phenomena are far outside the realm of laboratory experiments, there is a strong need to embed such simulations in a robust physics-based framework of these coupled dynamical systems.

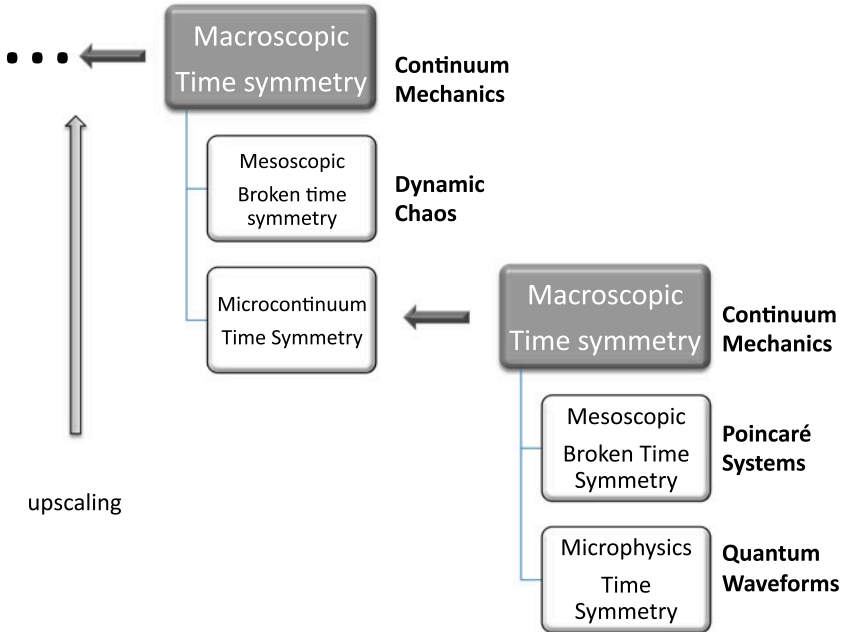

Figure 1. Time dependency becomes important when modelling the material behaviour in between scales. At the smallest scale quantum waveforms are time-independent; however, at larger scale their interactions lead to coupled oscillators with large Poincaré system behaviour as in the three body planetary system problem. These systems have complex trajectories and dynamic attractors [12]. Scaling up further the large Poincaré systems become continuous spectra and ultimately we recover the laws of classical continuum mechanics with time symmetry. We argue that similar space-time transitions occur multiple times in an Earth system, owing to the multiphysics processes of rock deformation. Phenomenological diffusion laws such as Fick, Fourier, Stokes, Navier allow assessment of the time-dependent behaviour in the region labelled dynamic chaos. These can be homogenized at even larger scale to form individual steady state time-symmetric structures that can be incorporated in continuum mechanics. The steady state dissipative pattern of the large scale homogenization from the smaller length scale diffusion process becomes the steady state micro-continuum of the next system defined by the next diffusional length scale in Equation (20) (see section on multiscale instabilities). More details on this topic can be found in Ref. [6].

5.1. *Solid mechanical instabilities*

Solid Mechanical instabilities can be seen as an elastoplastic bifurcation phenomenon in a time-independent framework. They are usually modelled using traditional concepts of mechanics, such as the bifurcation criterion involving the eigenvalues of the acoustic tensor, presented by Rudnicki and Rice [15]. This material bifurcation takes place when loaded at stress states near the yield stress, hence the elastoplastic plastic strain rate is given through the first term of the Taylor expansion of Equation (11) as:

$$\dot{\epsilon}_{ij} = \dot{\epsilon}^{e}_{ij} + \dot{\epsilon}^{in}_{ij} = C^{e}_{ijkl}\dot{\sigma}'_{kl} + \lambda_L \left\langle \frac{dy}{d\sigma_{ij}} \dot{\sigma}'_{ij} \right\rangle = C^{ep}_{ijkl}\dot{\sigma}'_{kl}, \tag{13}$$

where $\langle \cdot \rangle$ are the Macaulay brackets and λ_L a Lagrange multiplier.

A homogeneous material subjected to loading develops a localization band for condition in the eigenvalue problem

$$\xi_{jk} u_k = 0, \tag{14}$$

where $\xi_{jk} = n_i C^{ep}_{ijkl} n_l$ is the acoustic tensor, n_i is the unit vector normal to the surface of discontinuity, and u_k is the eigenvectors.

5.1.1. *Steady state (Time-symmetric) shear band width*

The original, above-described, bifurcation analysis defines localization bands which in the classical slip line field approach have vanishing thickness [16]. This drastic idealization has been removed by considering internal material length scales such as they arise for example at the small scale from the energetics of grain rotations [17]. In this case, a shear zone of finite width L can be derived from Cosserat continuum theory. We argue that similar energy-based internal length scales can be derived from the steady state limit of phenomenological diffusion equations (Fick, Darcy, and Fourier) of the individual microprocesses considered. Since the diffusivities are orders of magnitude apart, we obtain a hierarchal system of shear zones within shear zones (Figure 2), where each system can for the sake of simplicity be described by a dual material behaviour, i.e. solid (elastic) outside of the shear zone and fluid (viscoplastic) inside the shear zone. This drastic simplification is justified considering the vast separation of material length and time scales.

In order to derive the energetics of the steady state width of shear bands we have to however, abandon the classical time-symmetric approach to localization phenomena and understand what governs the evolution of the micro processes inside the shear band as a function of the full time dependent fluid dynamic elasto-viscoplastic processes.

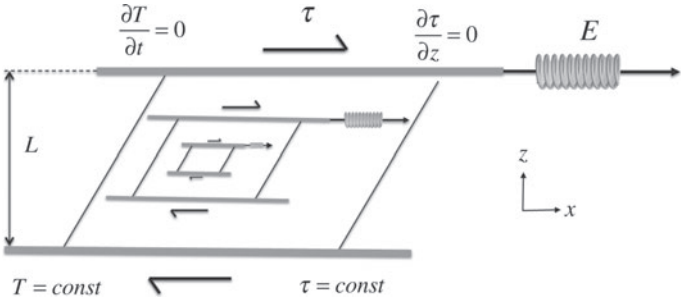

Figure 2. Simple nested solid mechanical-fluid dynamical (Babushka-style) identification of multiphysics, multiscale instabilities for the example of instabilities in shear (the same scheme can be transferred to volumetric dilatant or compactive instabilities [18]). The macro-scale solid mechanical view of the shear zone treats the outside view and is time-independent assuming isothermal conditions on the boundaries of the shear zone. It also assigns continuity of stress across the shear zone (i.e. $\tau = const$). The macroscale (solid mechanical) solution is incognisant of the internal processes in the shear zone and the internal length L has to be assigned. This length can only be evaluated from the internal time-dependent fluid dynamic view of the processes. Owing to the vast separation of length scales and time scales of the multiphysics time-dependent feedback processes, we suggest to identify only the dominant physics controlling the diffusional length scale L of the investigated scale. From the inside (fluid dynamic) time-dependent perspective, any outside deformation process occurs at time scales that are too slow to be considered and the outside domain can be regarded as elastic.

5.1.2. *Fluid dynamic (Broken time symmetry) instabilities*

We consider the fluid dynamic evolution of the shear zone by considering explicitly the temperature sensitivity of creep in Equation (12) and paramaterize the problem by the thermally activated constitutive equation:

$$\dot{\epsilon}_{ij}^{vp} = \dot{\varepsilon}_0 f(\sigma_{ij}) e^{-T_0/T}, \tag{15}$$

where T_0 is the activation temperature. Assuming further for simplicity that all of the mechanical power is converted into and no additional heat source or heat sink is available. It follows that the shear heating term is:

$$\delta_{loc} = \sigma_{ij} \dot{\epsilon}_0 f(\sigma_{ij}) e^{-T_0/T}. \tag{16}$$

Using a coordinate system moving with the material we obtain from Equation (8):

$$\frac{\partial T}{\partial t} = \frac{\partial^2 \kappa T}{\partial z^2} + \frac{\delta_{loc}}{\rho C}. \tag{17}$$

This equation is well known in combustion theory [14] as the solid-fuel model and features blow up instabilities at a critical value of δ_{loc}. Gruntfest [19] first recognized the importance of this instability for the temperature-sensitive viscous flow problem. Because of the catastrophic runaway instability this equation becomes unstable at a critical dissipation. It can be stabilized by reconsidering in addition the energy term from Equation (8) that buffers the runaway instability and acts as an endothermic energy sink,

$$\frac{\partial T}{\partial t} = \frac{\partial^2 \kappa T}{\partial z^2} + \frac{\delta_{loc}}{\rho C} - \rho T \frac{\partial^2 \psi}{\partial T \partial \alpha^k} \dot{\alpha}^k. \tag{18}$$

In the simplest case, this energy sink could be melting thus limiting the runaway and the energy sink would then be the latent heat of melting or an endothermic chemical reaction [20]. When introducing this term, the solid-fuel cell becomes an energy oscillator equation for critical dissipation. It features long periods of stable creep and short bursts of accelerated creep (Figure 3). This oscillatory behaviour is found to apply to all types of multiphysics instabilities, whether it is a small-scale chemical reaction [21] or a large-scale shear heating cycle [22].

In order to transform this oscillatory time-dependent fluid dynamic problem into a time-independent solid mechanical problem, we are interested in the steady-state (time symmetric) response where the temperature does not change. Hence, we set $\frac{\partial T}{\partial t} = 0$ and also set $\kappa = const$ and obtain:

$$-\kappa \frac{\partial^2 T}{\partial z^2} = \frac{\delta_{loc}}{\rho C}. \tag{19}$$

We are left with the steady-state solution where the heat produced by the oscillator is in equilibrium with the heat diffusion away from the shear plane. This partial differential equation recovers the familiar error function solution for the diffusing heat front and the shear zone has the characteristic diffusive scaling length [23,24]:

$$L = 2\sqrt{\kappa t_{cr}}, \tag{20}$$

where the time t_{cr} derives from the critical shear heating value for switching on the energy oscillator. We have now derived the internal scaling length of the shear zone and can formulate a time-independent plasticity law where we replace the energetic instability criterion

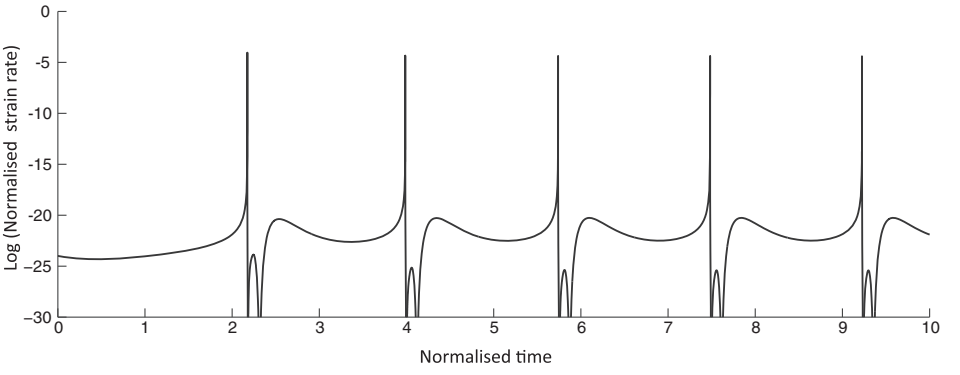

Figure 3. Generic illustration of the energy oscillator equation for critical dissipation. The strain rate shows cycles of fast acceleration (note log scale) and locks into periodic creep bursts interrupted by long periods of low background creep. This oscillator forms an energy attractor and is reached irrespective of the initial conditions. Figure reproduced with permission from AGU [21].

by a critical hardening parameter [15,25] for the onset of localization. The equivalence between fluid and solid mechanical solution is obtained if at steady state limit, the actual value of stress is recovered from the fluid dynamic solution and the hardening parameter is set smaller than the onset of instability for shear heating values that are insufficient to create an instability. The hardening parameter is set to critical for shear heating values sufficient for onset of instability.

It can be shown [2,3] that the same style of diffusion length scaling in Equation (20) occurs for all styles of instabilities described by the solid-fuel model (Equation (17)) or similarly for the more complete energy oscillator equation (Equation (18)). This covers the general class of thermo-hydro-mechanical-chemical THMC instabilities. Because there is a vast separation of diffusivities, a strong separation of space-time instabilities is derived which makes the simplification shown in Figures 1 and 2 very powerful. TMC feedback processes show instabilities below millimetre length scale while THM occupy the length scale of *cm–m*. The pure TM process described above has a typical length scale between hundreds of meters and several kilometres [2,3].

The time scales for instabilities are also vastly different. Peculiarly, the longest time scale is covered by the TMC (not the short-time scale THMC) feedback which can be on the order of million years because the rates of chemical reactions are extremely slow at the low temperatures of geological problems. This pairing of the smallest length scale with the shortest time leads to a tight (parallel) coupling of geodynamic scale processes with micro-structural processes. Therefore, any geodynamic solution must indeed incorporate consideration of the local chemical state such as shown for the problem of subduction initiation [26]. The intricate coupling of chemistry with long wavelength processes is already known through elastic coupling. Elastic properties of polymineralic rocks can simply be calculated for a given chemistry under a given pressure and temperature using the averaging of the stoichiometry coefficients and minimizing Gibbs free energy [27]. We extend this equilibrium thermodynamic framework to far from equilibrium processes and use the non-linear nature of the energy oscillator to advantage to avoid complete tightly coupled nano-km scale simulations. In simple terms, chemical reactions can be chosen to act like a switch for

a given level of dissipation. Either the chemical/microstructural ingredient is not present and the TM instability is occurring for extreme conditions outside the realm of geodynamic forcing or the critical chemical ingredient is present and its activation temperature has been reached so that instability occurs.

The other processes are less complicated. TM covers typically hundred thousand years – several years, whereas THM has relatively short timescales of seconds to weeks [2,3]. A direct outcome of this time separation and the formalism suggested in Figure 1 is that a solid that on the long TMC timescale must be regarded as a creeping solid becomes an elastic solid for the time scale of the TM and the THM process. This concept is best illustrated in a working example.

6. Worked case study

For the worked case study, we consider an unsolved problem in geodynamics, i.e. that of intraplate tectonics. Plates are defined to be rigid so that they can rotate on Euler poles and accommodate the convection currents in the Earth's mantle. To first order, there are only three elements that disrupt the postulate of rigidity, namely great circle sources of material which form the Mid Ocean Ridges, great circle sinks which form the oceanic subduction zones and oceanic transform faults which accommodate the shear on small circles around the Euler poles. Together, this information allows the identification of the Euler vectors of plate motion. Continents are thought to be to first-order passive fragments that are pushed around by the large-scale oceanic motions and incompatibilities are accommodated in continental collision zones leading to mountain building processes, the so-called great orogenies. Why then is it possible to have intraplate orogenies in the middle of a strong and old (= craton) continental plate?

One of the world's largest sedimentary basins, the Centralian Superbasin in Australia, was developed in the continental interior by long-lived slow subsidence and without a parent response to lithospheric stretching. Subsequently, the basin became the locus of crustal-scale shortening, giving rise to two intraplate orogenic belts, 570–530 Myrs Petermann orogeny and the 370–300 Myrs Alice Springs orogenies. In the sections to come, we present numerical modelling results that demonstrate that far-field compression can give rise to the formation of large-scale sedimentary basins associated with downwarping of the weak, ductile and dense part of the lithosphere, underneath a strong elasto-viscoplastic, mid-crustal core.

Our model is based on thermomechanical coupling, large transformations of continua, viscoplastic rock behaviour and continuum damage mechanics. The damage mechanics approach is the important component that receives and averages information gained through a high-resolution synchrotron X-ray tomographic analysis of deformed granites exposed through the orogeny. The sample from the Redbank shear zone clearly illustrates the important role of mid-crustal fluids that are released through a dissolution-precipitation reaction causing creep fractures through cavitation on the grain boundaries [28,29].

These mechanisms are combined in a self-consistent thermodynamic framework which allows for out of equilibrium description of the material behaviour. In the following analysis, we investigate whether the Centralian Superbasin profile can be understood as a non-linear response to a monotonic compression resulting in length and time scales which are directly related to the geometry, rate dependency, rigidity and strength and temperature distribution.

6.1. *Geological observations*

Intracratonic sedimentary basins and intraplate orogenies are two global-scale tectonic features that are still relatively little understood. Intracratonic basins are large (>150,000 km^2 in area) sedimentary basins that developed within the continental interior over an extended period (>200 Myrs) of subsidence. Such basins formed on an old continental lithosphere away from any known active tectonic margin [30,31] and are commonly floored by thick continental crust and lithosphere [32,33]. The absence of crustal thinning beneath intracratonic basins means that models attributing their development to lithospheric extension are somewhat tenuous [34].

The existence of intraplate orogenies is equally puzzling. These represent crustal-scale zones of localized strain within continental interiors, thus contradicting the 'rigid' behaviour of tectonic plates as implied from the plate tectonic theory. Why does localization occur in the continental interior rather than in the 'weak' boundaries and how the stresses transmitted through the lithosphere still remain open questions [35,36].

Central Australia provides an excellent example of an intracontinental basin that subsequently became the locus of intraplate strain localization. N-S shortening deformation occurred during two extended periods, related to low background compressive strain rates [35] and resulted in crustal-scale reverse faulting that has offset the Moho and produced one of the world's largest gravity anomaly [37]. Some authors have attributed this localization to reactivation of pre-existing weak structures [38], whereas others suggested that thermal weakening associated with the sedimentary blanketing played a major role [39]. Both scenarios are possible, but in practice the latter form of perturbation is more attractive as it is more naturally achievable in a system which is a priori stable in terms of initial conditions.

Therefore, we explore the geodynamics of intraplate deformation under a simple compression scenario together with a small thermal perturbation. The thermomechanical coupling, the dissipative processes (thermal feedback, damage, plasticity and visco-plasticity), the plain-strain spherical geometry, as well as the simple loading scenario that we selected produce similar patterns of deformation as those observable in the field. Previous attempts to explain the Centralian Superbasin have well been aware of their shortcomings. Lambeck [40] found that the basin resembles that of an elastic buckling instability of the interior of the Australian plate (see Figure 4), but he concluded that the stresses to achieve such buckling would be far too high. An alternative model where significant intraplate weaknesses are assumed to enable reactivation [36] clearly stated that while the mechanism works, it is assumed a priori and it is unclear what essentially causes these zones of decreased lithospheric strength.

Here we attempt to solve the problem by consideration of thermomechanical coupling within the above-discussed self-consistent thermodynamic framework to investigate whether chemical weakening through dissolution-precipitation creep can affect global tectonics. We consider a spherical Earth with realistic plate-scale dimension and apply low tectonic driving force on the plate margins, thus achieving low deformation rates [35]. We show that long-lived compressional stresses, transmitted from the plate boundaries, can explain the origin of intracratonic sedimentary basins as compressional basins. Furthermore, we show that strain can be localized in the form of buckling instabilities thus explaining intermittent formation of intraplate orogens.

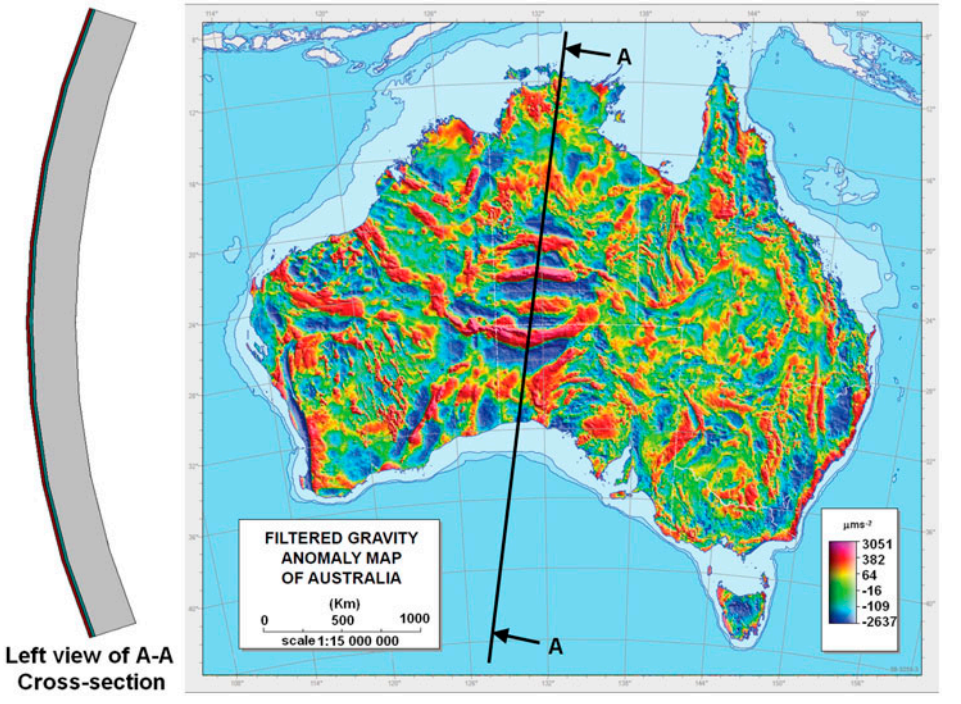

Figure 4. (colour online) Gravity map showing the strong anomaly reminiscent of a lithosphere buckling signature [40], the Alice spring region and the cross section to be modelled.

6.1.1. *Geological setting*

The Centralian Superbasin in central Australia is a large sedimentary basin that developed during a long-lived (approx. 500 Myr) history (from 800 Myrs) of subsidence and widespread sedimentation [39,41]. It comprises a number of basins (Officer, Amadeus, Ngalia, Georgina and Wiso basins), which are separated from each other by inliers of metamorphic complexes uplifted during intraplate orogenies. The formation of the Centralian Superbasin was interrupted by two major intracratonic orogenic episodes. These include the 570–530 Myrs Petermann orogeny and the 370–300 Myrs Alice Springs orogeny [41–43]. Both orogens expose deep crustal rocks in their cores [37,44] and involved large offsets in the crust-mantle boundary caused by N-S shortening [37,40].

Geophysical observations, particularly gravity, indicate that the crust is considerably thicker under the basins than it is under the regions where basement rock is exposed [45] and thinner underneath the two orogenies. This is supported by Ar-Ar thermochronology, which suggests that the thickest parts of the superbasin occurred over the now exhumed basement rocks [39]. This suggests that the orogenic structures were not necessarily controlled by local, pre-existing weak faults [36,38] but rather involved a larger scale phenomenon. Thermal weakening due to the presence of heat-producing elements under the thick sedimentary cover has been suggested as a contributing factor [35].

6.1.2. *Identifying basic physics, nanoscale, nm–mm*

Rather than postulating ad hoc weakening laws, we follow here the multiscale, multiphysics strategy laid out above and try to identify the physics/chemistry of the processes driving the instabilities. We refer to an earlier study where deformed samples exposed through the Alice Springs orogeny in the Redbank shear zones were analysed with high resolution Synchrotron X-ray micro-tomography, NanoSims and SEM measurements [29]. These micro-tomograms of host rock and shear zone reveal the formation of a dynamic mode of interconnected porosity network in the most highly strained section of the deformed sample. The chemical analysis showed that the key mechanism of deformation is based on a dynamic porosity generation through THMC feedback with following basic dissolution-precipitation reaction where K-feldspar plus H^+ dissolves into Muscovite plus K^+ and Quartz in aqueous solution,

$$3KAlSi_3O_8 + 2H^+ \leftrightharpoons KAl_3Si_3O_{10}(OH)_2 + 2K^+ + 6SiO_2(aq). \tag{21}$$

It is beyond the scope of this paper to describe how this fully coupled THMC feedback mechanism is upscaled into the simpler T(C)M damage mechanics approach for geodynamic modelling. For a more complete account, we refer to Ref. [46] and focus here on the description of the large-scale simulation where we have to consider finite strain owing to the large deformation.

6.1.3. *Constitutive approach, large scale, >10 km*

We make use of the classical (1-D) theory of damage mechanics, which has been extensively used over the past decades for applications in metal and ceramics deformation. In these materials, the phenomena described in nanoscale characterization of granites are well-known and void nucleation, growth and coalescence has been modelled via a damage mechanics approach. The first work (see [47] for a review) proposed a plastic potential taking into account both the void nucleation and growth. We make use of the subsequent development based on the concepts of Lemaitre [48] and Chaboche [49] who formulated a thermodynamic framework and suggested numerical schemes capable of predicting the degradation of the materials.

In analogy to Equation (2) and following we postulate for a finite strain formulation a Helmholtz free energy of the form $\psi(h^e_{ij}, T, D)$, where $h^e_{ij} = Ln(\frac{1}{2}F^e_{ki}F^e_{kj})$ is the Hencky strain measure of elastic strain, F^e_{ij} is the elastic gradient of deformation, T is temperature and D is a scalar which accounts for material degradation (damage). We also make use of the Clausius–Duhem inequality along with the technique of independent processes introduced by Ref. [50] to obtain the following relationships:

$$\tau_{ij} = \rho_0 \frac{\partial \psi}{\partial h^e_{ij}} \text{ (a)}, \quad \mathrm{Y} = \rho_0 \frac{\partial \psi}{\partial D} \text{ (b) and } \mathrm{s} = -\frac{\partial \psi}{\partial T} \text{ (c)}, \tag{22}$$

where τ_{ij} is Kirchhoff stress and Y is the thermodynamic force of damage. Equation (22) shows that the form of Helmholtz free energy is crucial in a thermodynamic analysis, it relates the state variables to the stored energy. Combined with the theorem of Schwartz about mixed partial derivatives, this free energy allows writing the following expressions:

$$\frac{\partial^2\psi}{\partial D\partial h^e_{ij}} = \frac{\partial^2\psi}{\partial h^e_{ij}\partial D}, \quad (a)$$

$$\frac{\partial^2\psi}{\partial T\partial h^e_{ij}} = \frac{\partial^2\psi}{\partial h^e_{ij}\partial T}, \quad (b) \tag{23}$$

$$\frac{\partial^2\psi}{\partial D\partial T} = \frac{\partial^2\psi}{\partial T\partial D}, \quad (c)$$

provided that $\psi(h^e_{ij}, T, D)$ is continuous and the second derivatives exist. Equation (23) summarizes the complexity of thermo-coupling in damageable materials. None of the off diagonal terms can be considered while ignoring its dual. For instance, if thermal expansion is recognized as an important contribution to Helmholtz's free energy and the damage parameter varies with external loading, then it is necessary to consider the coupling between damage and temperature as well. As we are interested in the materials behaviour at finite strain, we express Helmholtz free energy in terms of the non-linear Hencky tensor. We first make use of the material isotropy at given temperature and damage and express the free energy with respect to the three invariants $I_1^{'}$, $I_2^{'}$, and $I_3^{'}$ of the Hencky tensor as follows:

$$\rho_0\psi(h^e_{ij}, T, D)\Big|_{T,D} = \omega_h(I_1^{'} = (h^e_{ii}), I_2^{'} = (h^{e\,2}_{ii})/2, I_3^{'} = h^{e\,3}_{ii}/3). \tag{24}$$

Hence, at given temperature and damage, we follow the derivations of Simo [51], who conducted a similar procedure to express hyperelastic material behaviour in terms of right Cauchy-Green tensor, to identify:

$$\rho_0 \left.\frac{\partial\psi}{\partial h^e_{ij}}\right|_{T,D} = \frac{\partial\omega_h}{\partial I_1^{'}} + \frac{\partial\omega_h}{\partial I_2^{'}}h^e_{ij} + \frac{\partial\omega_h}{\partial I_3^{'}}h^{e\,2}_{ij}. \tag{25}$$

We develop the energy potential to the second order: $\omega_h = \tau_0 I_1^{'} + \lambda(I_1^{'})^2/2 + 2\mu I_2^{'} + O(\|h\|\,2)$, to derive the following relationship:

$$\rho_0 \left.\frac{\partial\psi}{\partial h^e_{ij}}\right|_{T,D} = p_0 + \tilde{\lambda}\, h^e_{ii} + 2\tilde{\mu}h^e_{ij}. \tag{26}$$

This relationship is similar to Saint Venant-Kirchhoff model except that it is expressed in terms of Hencky tensor instead of Lagrange-Green tensor. The coefficients $p_0, \tilde{\lambda}$ are the initial stress and the Lamé constants. Combining Equations (22) and (26) results in the hyperelastic constitutive equation:

$$\tau_{ij} = \tilde{\lambda}\, h^e_{ii} + 2\tilde{\mu}h^e_{ij}. \tag{27}$$

Using the concept of effective stress to describe the material degradation due to external loading, (see for instance Ref. [52]), Equation (27) can be redefined in terms of the damage variable D and the Lamé parameters of the non-damaged material as follows:

$$\tau_{ij} = (1-D)\lambda\, h^e_{ii} + 2(1-D)\mu h^e_{ij}. \tag{28}$$

Combining Equations (22(b)), (23(a)) and (28) results in the relationship

$$Y = -\frac{\tau^2_{eq}}{2E(1-D)^2}\left[\frac{2}{3}(1+\nu) + 3(1-2\nu)\left(\frac{\tau_H}{\tau_{eq}}\right)^2\right]. \tag{29}$$

Further details on the damage approach and its application to geology can be found in [53,54]. Note that in our calculations, we arbitrarily limited damage to the conditions $D \leqslant 0.85$. This avoids the singularity for D going to unity and honours the fact that in geological materials (through processes that have not been considered in our simple model), shear zones retain mechanical strength even when highly damaged.

Thermodynamics therefore allows us to compile a frame indifferent formulation for finite strain where the energy material properties retain their meaning even for large deformation. For the co-rotational formulation of the stresses, we refer to the standard objective co-rotational stress rate,

$$\dot{\tau}^{o}_{ij} = \dot{\tau}_{ij} + \tau_{ik}\Omega_{kj} - \Omega_{ki}\tau_{jk}, \tag{30}$$

the difference being the definition of the logarithmic spin Ω_{ij} which has to be adjusted for a finite strain measure. Please refer to Ref. [53] for a full expression of the finite logarithmic spin.

Using the additive decomposition introduced in Equation (4), we can now define an intrinsic dissipation pseudo-potential $\phi(\sigma, Y)$ which contains a first term, $g_{(\sigma)}\sigma$, corresponding to inelastic deformation and a second term, $g_{(Y)}\sigma$, corresponding to damage. Following the rationale laid out in Equation (11), we incorporate the rate-dependency through a zero-valued condition of the form:

$$g_{(\sigma)}\sigma + g_{(Y)}Y - \tilde{\phi}\dot{\epsilon}^{in} = 0, \tag{31}$$

where $\tilde{\phi}$ is an invertible function relating the rate of equivalent inelastic deformation to the equivalent stress and $\tilde{\phi}^{-1}$ is its inverse. These considerations lead to flow rules of the form:

$$\dot{\epsilon}^{in} = \lambda_L \frac{\partial g_{(\sigma)}}{\partial \dot{\epsilon}^{in}} \text{ and } \dot{D} = \lambda_L \frac{\partial g_{(Y)}}{\partial Y}, \tag{32}$$

where λ_L is a Lagrange multiplier. In addition, from the Taylor expansion in Equation (11), the yield function can be decomposed into athermal and thermal terms as follows:

$$f(\sigma) = \frac{\sigma_{eq}}{1-D} - Y_a - \tilde{\phi}^{-1}\dot{\epsilon}^{in}_{eq}, \tag{33}$$

where Y_a is the thermal yield stress.

In this study, the rate-dependent mechanisms of the undamaged matrix are derived from experiments [55,56] that are often used for geodynamic simulations e.g. Ref. [26,57]. These simulations assume that diffusion and dislocation creep can adequately describe the rate-dependent deformation of materials under different levels of loading and environmental conditions. The Arrhenius equation is used to describe the resultant rate of strain of each mechanism with the generic equation:

$$\dot{\epsilon}_m = A_m \sigma^n_{eq} e^{-\frac{Q}{RT}}, \tag{34}$$

where the subscript m denotes the creep mechanism, A_m is a multiplicative constant, Q_m the activation energies and R the gas constant. The material constants and the power law exponent n are experimentally derived in the laboratory and their references and values are listed in Table 1.

The individual creep mechanisms can act simultaneously in the deforming matrix and their combination can be performed by expressing the viscoplastic overstress $\tilde{\phi}$ in terms of the over-stresses of the individual mechanisms. Thermomechanical loading of the

matrix causes rearrangements of point and line defects and crystals produce measurable macroscopic strains.

Although fundamentally different from defects, voids can contribute to the overall macroscopic strain in a similar manner and transfer fluids by the above-described dissolution-precipitation reaction. Expressing the equivalent inelastic deformation $\dot{\epsilon}^{in}$ in terms of Lagrange multiplier λ_L and adding a damage nucleation function $\eta(Y)$, which depends on the thermodynamic force of damage to Equation (29), it follows that

$$\dot{D} = \left((1-D)^{-(n+1)} + \eta(Y) - 1\right)\lambda_L. \tag{35}$$

Therefore, using the expression $\dot{D}$ (see first section), the damage potential we are searching for is: $g_Y = \left((1-D)^{-n+1} - 1\right)Y + \aleph(Y) + c$, where $\aleph$ is the integral of η and c is a constant of integration.

The above-described large-scale formulation allows us to tackle previously unsolved plate tectonic problems with a fresh approach. We now come back to the problem of Superbasins and intraplate orogenies in the interior of the Australian plate. We show that the geological observations can be explained by the consideration of application of a long-term compressive load over hundreds of million years on the Australian continent.

6.1.4. *Model setup, >10 km scale*

The initial configuration of the Australian continent is modelled with a plain strain cross section of a spherical earth with equally partitioned upper and lower crust of depths 20 km and a mantle of depth 260 km (see Figure 5). The whole cross section, which has an external radius of 6400 km, covers differential latitude of 40°. An initial geostatic stress state was established in the model using a gravity force $g = -9.8e_r$. The body force is expressed in a polar system of coordinates (e_r, e_θ) with a pole which coincides with the centres of the coaxial arcs and a polar axis which coincides with the geometrical axis of symmetry. An initial temperature profile is chosen that follows a geotherm that is thermodynamically consistent with P and S-wave velocities [58]. This profile consists of a gradient of 15°/km in the crust and 3°/km in the rest of the lithosphere.

As a constant load, the cross section is subject to circumferential body forces applied on the left and right sides of the model. Their integral with respect to volume coincides with the ridge-push obtained from classic plate tectonics theory [59] :

$$\left\| F_{rp} \right\| = \int_S \rho \left\| F_\theta \right\| dS = \frac{\theta a}{3R} \sum_{n=1}^{N} \rho_n \left(R_n^3 - R_{n-1}^3 \right), \tag{36}$$

where ρ_n is the density and R_n is the external radius of a given layer indexed by n. The above force has a magnitude $F_{rp} \approx 10^{12}\mathrm{Nm}^{-1}$ provided that the control parameter is $a \approx 10^{-3}\mathrm{ms}^{-2}$. While constrained by the above-mentioned constant external forces from both sides, the cross section is allowed to slide from the bottom as shown by the rollers in Figure 5. The material properties used for the simulation are detailed in Tables 1 and 2 for each of the three layers: the thermo-elastic properties of the upper crust are averaged using a mixture of quartz and feldspar, those of the lower crust are modelled with the elastic characteristics of feldspar, and the mantle is modelled using the thermo-elastic properties of olivine. Elastic properties are taken from Ref. [60]).

Table 1. Thermo-elastic properties used for simulation.

Layers	Upper crust	Lower crust	Mantle
Density (kg/m^3)	2800	2800	3200
Bulk modulus K (GPa)	34	84	128
Shear modulus G (GPa)	20.4	40	82
Thermal expansion (K^{-1})	1.3×10^{-5}	1.11×10^{-5}	2.21×10^{-5}
Heat capacity (Jmol$^{-1}K^{-1}$)	40.0	241.48	124.54

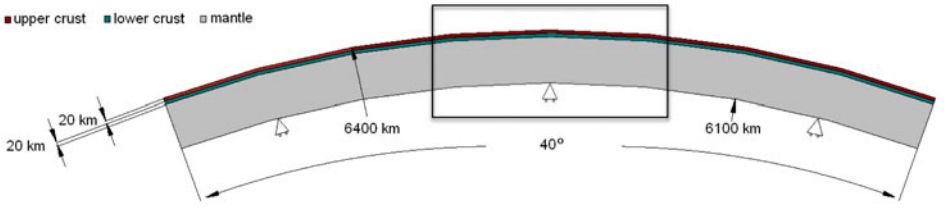

Figure 5. (colour online) Geometry of the model (dimension of the cross section). Only the central portion (box) is shown in the following results.

Table 2. Visco-plastic properties of the three layers. The creep parameters of the three layers are described by Ref. [61] for the upper and lower crust and by Refs. [55,56] for the mantle.

Layers		Upper crust	Lower crust	Mantle
Pre-coefficient A(MPa $-$ ns$^{-1}\mu$m^{3*})	Diffusion	3.1×10^{-4}	3.5×10^{-3}	4.8×10^{4}
	Dislocation	–	–	1.5×10^{3}
Exponent n	Diffusion	2.2	3.2	1.1
	Dislocation	–	–	3.0
Activation energy Q(kJ mol^{-1})	Diffusion	190	238	295.0
	Dislocation	–	–	470.0
Activation volume (m^3 mol^{-1})		–	–	20×10^{-6}
Grain size (μm)		–	–	15
Yielding limit Y_a^0 (MPa)		51	100	202

Since the materials considered in the three layers can undergo high differential stresses at high temperatures, we also considered the visco-plastic behaviour of the materials with rate dependency governed by dislocation creep in the upper and lower crust and by combined dislocation and diffusion creep mechanisms in the mantle. Table 2 summarizes the limits of elasticity that we considered as well as the creep mechanisms.

In accordance with the experimental results conducted by Ref. [62] on quartz at high temperature, the limit of elasticity is taken to be temperature dependent. A best fit of the form: $Y_a = Y_a^0 \exp(-(T - T_{\text{ref}})/A)$, where A = 305 K, was used to describe this dependency.

In order to mimic the natural aspect of geological materials, random weaknesses were distributed in the three layers. Random elements are selected in space, in such a way that 10%

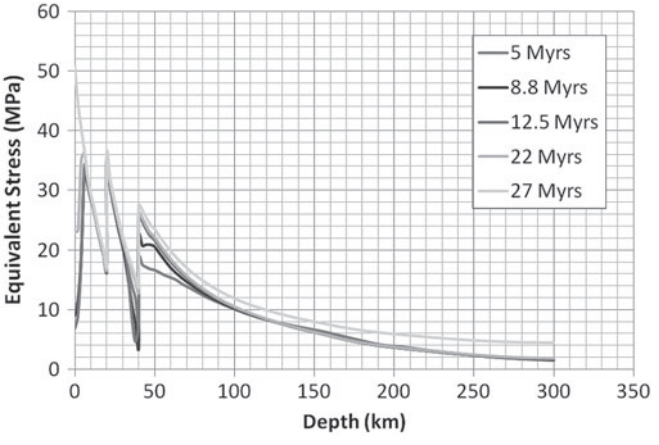

Figure 6. Evolution of the lithosphere strength profile from around the onset of the first buckling instability.

of the domain contains perturbations. A given perturbation consists in reducing the elastic and yielding properties by 0 to 10% of their original value. Note that both the position of the weaknesses and the reduction of the properties follow uniform probability distributions.

We first examine the response of the materials in terms of equivalent stress in the initial elastic deformation dominated regime at the onset of loading. Figure 6 shows the variation of the equivalent stress profile with respect to depth and time. Before the onset of the first long wavelength buckling instability in the first 12.5 million years, there are negligible variations of the equivalent stress profile with respect to time. The onset of bifurcation is identified in the strength profile when the equivalent stress increases in the upper mantle from 18 to 22 MPa. This increase is not a sudden event, but a continuum process which continues gradually, and relaxes with respect to time as the deviatoric stress seems to equilibrate at a depth of 50 km; the different curves approach each other progressively when time reaches 12.5, 22.5 and 27 million years. The figure also shows that the overstress propagates towards the surface of the cross section as can be seen from the peak that is reached in the upper crust at about 27 million years. This analysis shows that although we are still in the dominantly elastic loading regime (no significant inelastic strain), the bifurcation is initiated by a time-dependent process which involves not only large thermo-hyperelasticity, but also visco-plasticity which affects the relaxation time and the stress propagation through the different layers of the lithosphere. Once the bifurcation is initiated, the increase of stresses produces high permanent deformations within the three layers and damages their structure.

Figure 7 shows the onset of significant inelastic deformation when initial hinge collapse starts at 45.1 million years in the centre of the model. This doubly verging thrust is fully established at 48 Myrs. Due to the random perturbations which were distributed in the model, the damaged zone propagates asymmetrically through the three layers towards the surface. The direction of propagation is ascendant because the healing effect limits the material degradation at high temperatures. At 50 and 93.6 million years, two new damage zones are sequentially initiated in the crust reducing the wavelength of the buckling instability. It initially takes place 250 km away from the central part of the model and propagates

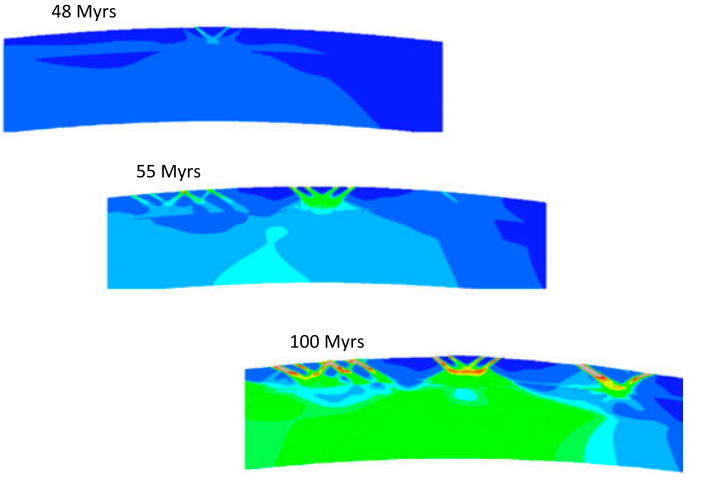

Figure 7. (colour online) Evolution of the buckling instability as a function of time showing inelastic strain (grey >100%).

towards the central detachment within the mantle. The progress of the left hand damage zone continues until a mantle detachment connects the left damage zone with the central one at 107.6 million years. As the steady state loading continues, a similar process takes place at 107.6 million years on the right hand side with the initiation of a new superficial weakness 236 km far from the axis of symmetry. The new damaged zone in its turn propagates through the three layers until it reaches the detachment within the mantle.

These results clearly illustrate the effect that damage accelerates weakening and increases inelastic deformation. It comes as no surprise that a damageable lithosphered allows intraplate buckling instabilities to occur as a natural outcome of intraplated stresses.

6.1.5. *Mesoscale, cm–km*

We are now shifting interest from the large-scale plate tectonic problem to the mesoscale regional field observations. At first, we will test the hypothesis from a macroscopic solid mechanical perspective. This implies that we are interested in comparing the natural width of the shear zones predicted by the large-scale model with nature. Our simple creep damage mechanics approach does not introduce an internal length scale. The only length scale present in the approach is the length scale for the diffusion of heat. We therefore expect from Equation (20) for a thermal diffusivity of $D = 10^{-6}m^2s^{-1}$ and a typical time scale defined by the inverse of the background strain rate $t = 10^{16}s$ a shear zone of the order of 10 km total width, which is also what comes out of the model calculation. This inference is slightly larger, but roughly matches with observations from field data and seismic inferences at depth [37] where the Redbank shear zone is described as a thrust zone of considerable lateral extent (7–10 km wide) with anastomosing mylonites [44] which dip at about 45° angle at outcrop level. Note that outcrops erode material that have formerly been deformed in upper greenschist facies conditions [29] that are around 400–500° C thus from around

20 km depth or deeper. The 45° angle of the thrust indicates the ideal direction of failure for a perfect von Mises body which is also expected from the model formulation at the given depth.

Another test for the shear heating hypothesis as a control of the width of the Redbank shear zone is to look into the internal structure of the shear zone. This implies looking at the problem from a fluid dynamic perspective and seeking to identify transient time-dependent structures inside the shear zone. The outside of the shear zone is simply viewed as an elastic spring (see Figure 2) and as we know that the system is post yield, we only need to solve the fluid dynamic shear heating problem. This leads directly to the energy oscillator equation. We expect from the energy oscillator Equation (18) intermittent, sharp heating events followed by long creeping periods as shown in Figure 3. The heating events are either buffered by chemical reactions such as the dissolution-precipitation reaction (Equation (21)) which limits the temperature rise due to the endothermic nature of the forward reaction, or by other energy sinks. An extreme case would be if there is no water available and the reaction cannot take place. In this case, one would expect for sufficiently high applied shear stress oscillatory sharp events where the temperature reaches local conditions for melting and the accelerated 'earthquake in the ductile domain' would cause cm-wide or smaller bands of molten rock. Such veins of pseudotachylyte have indeed been described in the paper of Hobbs et al. [44] who also originally proposed the model shown Figure 2 to explain these instabilities.

6.2. *Discussion*

We have presented two alternative simplifications of the multiscale, multiphysics approach that allow a staggered reduction of the problem to closed form analytic solutions for a given scale and a given time scale and system perspective. From a macroscopic perspective, the problem can be solved using a classical solid mechanical quasistatic approach where the simplified analytical solution technique is slip line field theory [16]. In the extreme rigid-plastic idealization, instabilities are velocity discontinuities with vanishing thickness but they are continuous in stress. The problem can be extended through an enriched continuum approach where a material length scale is added. The time-dependent processes inside the shear zone are not modelled.

From a microscopic perspective inside the shear zone, the problem can be viewed as a fluid dynamic problem and the overstress plasticity [13] problem is solved using the constant force applied by the load from the elastic spring on the outside as a boundary condition. The analytical solution of this problem [19] has identified a fundamental runaway instability (Equation (17)) known as the solid-fuel model of combustion physics [14]. A more realistic equation has been introduced that acknowledges thermally activated energy sinks and is here called the energy oscillator equation (Equation (18)). Asymptotic analytical solution for the multiple steady states are available [63]. Investigation of the transient behaviour shows that for a critical energy level (activated state), the system transients are found to be trapped into a thermo/hydro/chemo-mechanical oscillatory response [21] irrespective of their initial conditions. Perturbations or interferences of these oscillators lead to chaotic large Poincaré system behaviour [64]. At abstract level, the energy oscillators form microphysics engines and because of their cyclic behaviour can be integrated to overcome the path dependence of the problem [6].

We have also shown how the approach can be incorporated into a numerical solution using an additive thermodynamic approach. Note that the additive (serial) approach breaks down for strong-scale interaction and a parallel formulation should be preferred. We have presented a worked example where the numerical approach is tested in application to a geological problem. In this example, we may have solved a long-standing riddle of intraplate deformation. We have recognized that compressional basins and intraplate orogenies are intimately linked with the former being the precursor of the latter. Intraplate orogenies are found to result from buckling instabilities that occur diachronously and give rise to sequential formation of orogenies. The orogenies themselves initially develop at depth within the hinges of the buckles, and appear at the surface only later due to uplift and erosion.

We have used the creep fracture hypothesis identified through micro and nano-tomographic imaging of ultramylonites inside the shear zone [29] and cast it into a finite strain damage mechanics formulation. This efficiently solves the criticism of earlier models that either require excessive stresses [40] or need pre-existing weak structures [36] to cause similar intraplate structures.

An interesting outcome is that the mechanism only works for very slow strain rates relevant for an intraplate setting in a cratonic environment subject to long-term loading. Creep fractures become inefficient for fast loading conditions (see Figure 7 in Ref. [54]). This is clearly illustrated by the slow speed of the process (Figure 7) where a long wavelength buckling instability slowly develops over a time span of the order of tens to hundred million years into progressively shorter wavelength instabilities and altering the natural elastoplastic eigenmodes for the initial deformation problem.

The results may give a new perspective for explaining ubiquitous large-scale sedimentary basins that are widespread in the old cratonic lithosphere such as the Parana Basin in Brazil, the Siberian Basin (both located inside but at the edge of a craton) and the North American intracratonic Basin. These basins could be a natural expression of various stages of buckling of the Earth. Their difference in appearance could be simply a function of the geometry of the craton and the direction and duration of compressional loading. Future work is necessary to resolve this important finding.

Disclosure statement

No potential conflict of interest was reported by the authors.

Funding

This work was supported by the Australian Research Council [ARC Discovery grant number DP140103015].

References

[1] ICME, *Integrated Computational Materials Engineering: A Transformational Discipline for Improved Competitiveness and National Security*, The National Academies Press, Washington, DC, 2008.

[2] K. Regenauer-Lieb, M. Veveakis, T. Poulet, F. Wellmann, A. Karrech, J. Liu, J. Hauser, C. Schrank, O. Gaede and M. Trefry, J. Coupled Syst. Multiscale Dyn. 1 (2013) p.1.

[3] K. Regenauer-Lieb, M. Veveakis, T. Poulet, F. Wellmann, A. Karrech, J. Liu, J. Hauser, C. Schrank, O. Gaede and F. Fusseis, J. Coupled Syst. Multiscale Dyn. 1 (2013) p.2330.
[4] I. Collins and G. Houlsby, R. Soc. London A 453 (1997) p.1975.
[5] H. Ziegler, *An Introduction to Thermomechanics*, North Holland, Netherlands, 1977.
[6] M. Veveakis and K. Regenauer-Lieb, Curr. Opin. Chem. Eng. 7 (2015) p.40.
[7] K. Regenauer-Lieb, A. Karrech, H.T. Chua, F.G. Horowitz and D. Yuen, Philos. Trans. R. Soc. London A 368 (2010) p.285.
[8] L. Onsager, Phys. Rev. 37 (1931) p.405.
[9] G. Houlsby and A. Puzrin, *Principles of Hyperplasticity: An Approach to Plasticity Theory Based on Thermodynamic Principles*, Springer Verlag, London, 2006.
[10] T. Poulet, K. Regenauer-Lieb and A. Karrech, Tectonophysics 483 (2010) p.178.
[11] M. Veveakis and K. Regenauer-Lieb, Pure Appl. Geophys. 1 (2014) p.3159–3174. doi:10.1007/s00024-014-0835-6
[12] I. Prigogine, *Time, dynamics and chaos: integrating Poincare's 'Non-Integrable Systems'*, in *Nobel Conference XXVI*, U.S. Department of Energy, Office of Energy Research (DOE/ER); Commission of the European Communities (CEC), Lanham, Maryland. Vol. CONF-9010321-1, 1990, pp. 1–27.
[13] P. Perzyna, Adv. Appl. Mech. 9 (1966) p.243.
[14] C. Law (ed.), *Combustion Physics*. Cambridge University Press, New York, 2006.
[15] J. Rudnicki and J. Rice, J. Mech. Phys. Solids 23 (1975) p.371.
[16] R. Hill, *Mathematical Theory of Plasticity*, Oxford University Press, New York, 1950.
[17] H.B. Muhlhaus and I. Vardoulakis, Geotechnique 37 (1987) p.271.
[18] M. Veveakis and K. Regenauer-Lieb, J. Mech. Phys. Solids 78 (2015) p.231.
[19] I. Gruntfest, Trans. Soc. Rheol. 7 (1963) p.95.
[20] E. Veveakis, S. Alevizos and I. Vardoulakis, J. Mech. Phys. Solids 58 (2010) p.1175.
[21] E. Veveakis, T. Poulet and S. Alevizos, J. Geophys. Res. 119 (2014) p.4558–4582. doi:10.1002/2013JB010071
[22] P. Kelemen and G. Hirth, Nature 446 (2007) p.787. doi:10.1038/nature05717
[23] D.A. Yuen and G. Schubert, Geophys. Res. Lett. 4 (1977) p.503.
[24] D. Yuen, L. Fleitout, G. Schubert and C. Froidevaux, Geophys. J. R. Astron. Soc. 54 (1978) p.93.
[25] J.R. Rice, J. Geophys. Res. 80 (1975) p.1531.
[26] K. Regenauer-Lieb, D. Yuen and J. Branlund, Science 294 (2001) p.578.
[27] D. Siret, T. Poulet, K. Regenauer-Lieb and J. Connolly, Geotech. Acta 4 (2008) p.107. doi:10.1007/s11440-008-0065-0
[28] K. Regenauer-Lieb, D. Yuen and F. Fusseis, Pure Appl. Geophys. 166 (2009) p.1.
[29] F. Fusseis, K. Regenauer-Lieb, J. Liu, R. Hough and F. deCarlo, Nature. 459 (2009) p.974.
[30] W. Dickinson, *Plate tectonic evolution of sedimentary basins*, in *Plate Tectonics and Hydrocarbon Accumulation*, W. Dickinson and H. Yarborough, eds., Continuing Education Course Note Series, American Association of Petroleum Geologists, Tulsa, Oklahoma, 1976, p.1.
[31] X. Xie and P.L. Heller, Bull. Geol. Soc. Am. 121 (2009) p.55.
[32] C. Braitenberg and J. Ebbing, Geophys. Prospect. 57 (2009) p.559.
[33] D. McKenzie and K. Priestley, Lithos 102 (2008) p.1.
[34] J.J. Armitage and P. Allen, J. Geol. Soc. 167 (2010) p.61.
[35] M. Sandiford, Earth Planet. Sci. Lett. 201 (2002) p.309.
[36] J. Braun and R. Shaw, *A thin-plate model of Palaeozoic deformation of the Australian lithosphere: implications for understanding the dynamics of intracratonic deformation*, in *Continental Reactivation and Reworking*, Vol. 184, Geological Society, J. Miller, R. Holdsworth, I. Buick and M. Hand, eds., Special Publications, London, 2001, p.165.
[37] B.R. Goleby, R.D. Shaw, C. Wright, B.L.N. Kennett and K. Lambeck, Nature 337 (1989) p.325.
[38] A. Camacho, B.J. Hensen and R. Armstrong, Geology 30 (2002) p.887.

[39] S. McLaren, M. Sandiford, W.J. Dunlap, I. Scrimgeour, D. Close and C. Edgoose, Basin Res. 21 (2009) p.315.
[40] K. Lambeck, Geophys. Res. Lett. 10 (1983) p.845.
[41] M. Hand and M. Sandiford, Tectonophysics 305 (1999) p.121.
[42] W. Collins and C. Teyssier, Tectonophysics 158 (1989) p.49.
[43] R.D. Shaw, M.A. Etheridge and K. Lambeck, Tectonics 10 (1991) p.688.
[44] B. Hobbs, A. Ord and C. Teyssier, Pure Appl. Geophys. 24 (1986) p.309.
[45] B.R. Goleby, B.L.N. Kennett, C. Wright, R.D. Shaw and K. Lambeck, Tectonophysics 173 (1990) p.257.
[46] K. Regenauer-Lieb, A. Bunger, H.T. Chua, A. Dyskin, F. Fusseis, O. Gaede, R. Jeffrey, A. Karrech, T. Kohl, J. Liu, V. Lyakhovsky, E. Pasternak, R. Podgorney, T. Poulet, S. Rahman, C. Schrank, M. Trefry, M. Veveakis, B. Wu, D. Yuen, F. Wellmann and X. Zhang, J. Earth Sci. 6 (2015) p.2.
[47] V. Tvergaard and A. Needleman, *Elastic-viscoplastic analysis of ductile failure*, in *Finite Inelastic Deformations – Theory and Applications, IUTAM Symposium Hannover/Germany 1991*, Dieter Besdo and Erwin Stein, eds., Springer-Verlag, Berlin Heidelberg, 1992, p.3.
[48] J. Lemaitre, Comput. Methods Appl. Mech. Eng. 51 (1985) p.31.
[49] J.L. Chaboche, Nucl. Eng. Des. 105 (1987) p.19.
[50] B. Coleman and W. Noll, Arch. Ration. Mech. Anal. 13 (1963) p.167.
[51] J.C. Simo and R.L. Taylor, Comput. Methods Appl. Mech. Eng. 48 (1985) p.101.
[52] J. Lemaitre and J. Chaboche, *Mecanique des Materiaux Solides* [Mechanics of solid materials], Duond, Paris, 2001.
[53] A. Karrech, K. Regenauer-Lieb and T. Poulet, Int. J. Solids Struct. 48 (2011) p.397.
[54] A. Karrech, K. Regenauer-Lieb and T. Poulet, J. Geophys. Res. 116 (2011), art. no. B04205.
[55] S. Mei and D.L. Kohlstedt, J. Geophys. Res. 105 (2000) p.471.
[56] S. Mei and D.L. Kohlstedt, J. Geophys. Res. 105 (2000) p.457.
[57] K. Regenauer-Lieb, R.F. Weinberg and G. Rosenbaum, Nature 442 (2006) p.67.
[58] J.C. Afonso, G. Ranalli and M. Fernandez, Phys. Earth Planet. Inter. 149 (2005) p.279.
[59] L.D. Turcotte and G. Schubert, *Geodynamics*, 2nd ed., Cambridge University Press, Cambridge, 2002.
[60] L. Stixrude and C. Lithgow-Bertelloni, Geophys. J. Int. 162 (2005) p.610.
[61] G. Ranalli, Rheology and deep tectonics 40 (1997) p.1997.
[62] G. Hirth and J. Tullis, J. Geophys. Res. 99 (1994) p.11731.
[63] S. Alevizos, T. Poulet and E. Veveakis, J. Geophys. Res. 119 (2014) p.4558.
[64] T. Poulet, E. Veveakis, K. Regenauer-Lieb and D. Yuen, J. Geophys. Res. 119 (2014) p.4606.